Phase relations of a serpentine composition between 5 and 14 GPa: Significance of clinohumite and phase E as water carriers into the transition zone

Article *in* Contributions to Mineralogy and Petrology · March 2001

DOI: 10.1007/s004100000208

CITATIONS
100

READS
245

2 authors:

Roland Stalder
University of Innsbruck
89 PUBLICATIONS **1,989** CITATIONS

SEE PROFILE

Peter Ulmer
ETH Zurich
252 PUBLICATIONS **9,378** CITATIONS

SEE PROFILE

Contrib Mineral Petrol (2001) 140: 670–679
DOI 10.1007/s004100000208

Roland Stalder · Peter Ulmer

Phase relations of a serpentine composition between 5 and 14 GPa: significance of clinohumite and phase E as water carriers into the transition zone

Received: 4 May 2000 / Accepted: 15 September 2000 / Published online: 9 January 2001

Abstract Run products from high pressure experiments at 800–1,200 °C and 5–14 GPa (corresponding to depths of 150 to 420 km) on a serpentine bulk composition [close to $Mg_3Si_2O_5(OH)_4$] were analysed by optical microscopy, micro-Raman spectroscopy and electron microprobe. All charges exhibit strong chemical zoning. Fluid, melt and hydrous solids were mostly concentrated at the top, bottom and along the wall of the capsules. The central part of the charge was devoid of H_2O. Both fluid and hydrous magnesian phases exhibit a Mg/Si ratio higher than forsterite. In contrast, the centre of the capsule was enriched in SiO_2. The observed zoning can neither be explained by gravitational settling nor by a thermal gradient alone. Most likely the fluid was separated from the solids by surface forces and thereby established the chemical gradient by preferentially dissolving MgO. If strong chemical zoning is taken into account, the occurrence of more phases than allowed by the phase rule can be explained by separating the bulk into several domains of different bulk compositions. Results indicate that small amounts of F increase the stability field of clinohumite, $Mg_9Si_4O_{16}(OH,F)_2$, compared to OH-clinohumite in pure MSH previously reported. Clinohumite coexists with enstatite up to 975 °C at 5 GPa, and up to 1,100 °C at 12 GPa. At 14 GPa (close to the α/β-Mg_2SiO_4 transition) phase E becomes the most important water carrier. The new results indicate that clinohumite could be an important mantle mineral for transporting water into the Earth's transition zone due to its high thermal stability compared to other important water carriers such as serpentine and phase A.

R. Stalder (✉) · P. Ulmer
Institut für Mineralogie & Petrographie, Sonneggstrasse 5,
ETH Zentrum, 8092 Zürich, Switzerland
E-mail: roland.stalder@erdw.ethz.ch
Tel.: +41-1-6323179
Fax: +41-1-6321088

Editorial responsibility: V. Trommsdorff

Introduction

Large amounts of water have been released throughout the Earth's history to the surface by volcanic activity. The opposite process, the transport of water back into the Earth's mantle, cannot be observed directly, but its viability can be studied using high pressure experiments on the stability of hydrous phases in mantle rocks. Numerous OH-bearing phases, the so-called dense hydrous magnesian silicates (DHMS), have been observed as stable constituents in high pressure experiments performed in model mantle rocks over the last few decades (e.g. Ringwood and Major 1967; Yamamoto and Akimoto 1977; Akimoto and Akaogi 1980; Liu 1987; Kanzaki 1991; Luth 1995). The DHMS have been reviewed recently by Wunder (1998).

To be a potential water carrier in the Earth's mantle on a large scale, a hydrous phase must be stable in an assemblage containing forsterite and enstatite, i.e. in a mantle bulk composition. In the system $MgO–SiO_2–H_2O$ (a model system for the Earth's mantle) all phases with Mg/Si-ratios higher than forsterite cannot occur with forsterite and enstatite as long as a hydrous fluid is stable with forsterite. Similarly, all phases with a lower Mg/Si-ratio than enstatite are not relevant to the Earth's mantle as long as the join enstatite–hydrous fluid is stable. The chemography shown in Fig. 1 summarizes the compositions of hydrous silicates observed in experiments to 15 GPa. Chemical compositions and symbols are listed in Table 1. The composition of hydroxylated mantle rocks, indicated in Fig. 1, is such that the occurrence of clinohumite, chondrodite or phase A requires the join forsterite–fluid to be replaced by a join between enstatite and one of these phases. Similarly, the 10 Å phase can only occur in these compositions when the join enstatite–fluid is broken (Chinnery et al. 1999). Alternatively the local bulk composition of a portion of the mantle has to lie outside the triangle forsterite–enstatite–water; although this is in principle possible, here it is not considered to be a common feature in the ultramafic part of subducted slabs

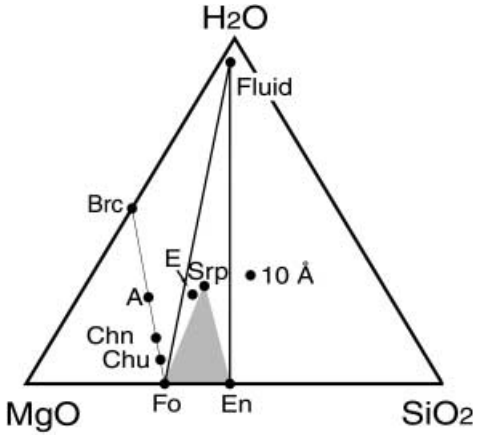

Fig. 1 Chemical compositions (in moles) of potential water carriers in the upper mantle as given in Table 1. *Srp* Serpentine, *A* phase A, *E* phase E, *10Å* 10-Å phase, *Chn* chondrodite, *Chu* clinohumite, *Brc* brucite; also shown: *Fo* forsterite and *En* enstatite. The composition of the fluid phase is illustrated schematically to indicate that its composition is not pure H_2O, because high pressure aqueous fluids can dissolve tens of wt% of silicate components (Stalder et al. 2000). The composition of hydrated mantle rocks plot within the *grey* triangle

and the overlying mantle. The storage of water in the subducted oceanic crust is not considered in this study.

At the onset of subduction of oceanic lithosphere water is stored mainly in serpentine-group minerals. Previous investigations (Luth 1995; Ulmer and Trommsdorff 1995; Bose and Navrotsky 1998; Irifune et al. 1998) inferred that only subduction along cool geothermal gradients (= 3 °C/km) would permit preservation of hydrous phases to depths exceeding 200 km. A 'choke point' located at approximately 6 GPa and 600 °C separates two different regions: a colder region where the breakdown of serpentine produces the assemblage enstatite + phase A, (and where H_2O is preserved in the solid assemblage), and a hotter region where serpentine breaks down to form forsterite + enstatite + fluid (where H_2O can no longer be transported in mineral phases). As a result H_2O would only be conserved in crystalline phases at the coldest area of the subducted slab.

Here we report results from high pressure–high temperature experiments in a multi-component system (close to MSH) carried out between 5 and 14 GPa and 800 and 1,200 °C. The study is focused on the stability of the DHMS phase A, phase E, OH-clinohumite and OH-chondrodite in an assemblage relevant to the Earth's mantle.

Experimental

As starting material we used a mixture of synthetic talc [$Mg_3Si_4O_{10}(OH)_2$] and brucite ($Mg(OH)_2$) with serpentine bulk composition [$Mg_3Si_2O_5(OH)_4$] containing approximately 1 wt% FeO, 0.5 wt% Al_2O_3, 0.1 wt% F and 0.02 wt% TiO_2. No phases other than brucite and talc could be identified by X-ray diffraction. The starting material was sealed in welded Au-capsules. Experiments were performed in a 6/8 multi-anvil apparatus using tungsten carbide cubes with truncation edge lengths (TEL) of 8, 11, 12 and 17 mm (Table 2). Stepped graphite heaters were used up to 9 GPa and stepped $LaCrO_3$ heaters were used at higher pressures. Au-capsules had an outer (inner) diameter of 1.6 (1.4) mm for the 8 mm TEL assemblies and 2.3 (2.0) mm for all other assemblies. Assemblies were calibrated at room temperature against the phase transition in Bi metal. High temperature calibrations are based on the following phase transitions: $CaGeO_3$: garnet–perovskite (6.0 GPa, 1,200 °C; Susaki et al. 1985); TiO_2: rutile/α-PbO_2 structure (7.7 GPa, 1,100 °C; Akaogi et al. 1992); SiO_2: coesite–stishovite (9.3 GPa, 1,200 °C; Yagi and Akimoto 1976; Zhang et al. 1996); Mg_2SiO_4: α–β-transition (14.5 GPa, 1,400 °C; Morishima et al. 1994). Temperatures were measured with Pt/PtRh thermocouples; reported temperatures are not corrected for the effect of pressure on the thermocouple emf.

To check for potential leakage the recovered capsules were weighed, pierced, dried and weighed again. As long as no hydrous silicates were produced during the run, 90–100 wt% of the water initially stored in the starting mixture was recovered after the run. Polished longitudinal cross sections were made from the run products; samples were examined under reflecting light microscope, and phases were identified by Raman spectroscopy (Dilor Labram2) and with an electron microprobe (Cameca SX50). Published Raman spectra of hydrous magnesium silicates are contradictory. Therefore, we synthesized phase A, phase E, clinohumite and chondrodite individually on their respective compositions. Run products were checked by electron microprobe and X-ray powder diffraction (details will be given in a separate paper, Ulmer and Stalder, in preparation). The Raman spectrum for phase A acquired by Hofmeister et al. (1999) corresponds to the spectrum of clinohumite obtained in this study (Fig. 2a). Our spectrum of phase A is identical with the spectrum of phase A reported by Liu et al. (1997a). The Raman spectrum of phase E published by Liu et al. (1997b) probably was derived from a forsterite crystal. In accord with Frost and Fei (1998), our phase E exhibits no sharp Raman-peaks. Instead, it shows characteristic broad bands at 500, 700, 950, 1130 and 3620 cm^{-1} (Fig. 2b, c). Phase E occurred – depending on temperature and pressure – in two different morphologies, one of which is interpreted to be a quench product (Fig. 3). Neither type of phase E shows any sharp Raman-peak, probably owing to its unique crystal structure.

In addition, X-ray powder diffraction patterns of some samples were recorded. However, due to coincidence with the strongest diffraction peaks of forsterite and enstatite, the detection limit of some hydrous phases such as clinohumite or phase E was rather poor. In run MSH46, phase E was identified by the following lattice spacings (Kanzaki 1991): 4.64 Å (003), 2.412 Å (012) and 2.067 Å (014).

Table 1 Compositions and abbreviations of phases in the MgO–SiO_2–H_2O system, including DHMS phases

Name	Abbreviation	Formula
Forsterite	fo	α-Mg_2SiO_4
Wadsleyite	wd	β-Mg_2SiO_4
Enstatite	en	$MgSiO_3$
Brucite	brc	$Mg(OH)_2$
Serpentine	srp	$Mg_3Si_2O_5(OH)_4$
10-Å phase	10 Å	$Mg_3Si_4O_{10}(OH)_2{\cdot}2H_2O$
Phase A	A	$Mg_7Si_2O_8(OH)_6$
Phase E	E	$Mg_{2.3}Si_{1.25}H_{2.4}O_6$
Chondrodite	chn	$Mg_5Si_2O_8(OH)_2$
Clinohumite	chu	$Mg_9Si_4O_{16}(OH)_2$

Results and interpretation of zoned capsule contents

Results are summarized in Table 2. In most run products four different phases could be identified. The

Table 2 Run details and results of quenching experiments. *TEL* truncation edge length. For abbreviations for phases see Table 1

Run	P (GPa)	T (°C)	Time (h)	Setup TEL (mm)	Phase assemblages
MSH49	5.0	900	48	25/17	Fo + En + Chu; En + Chu + Fluid
MSH51	5.0	975	24	25/17	Fo + En + Chu + Fluid
MSH48	5.0	1,050	18	25/17	Fo + En + Fluid
MSH55	6.0	800	72	19/12	Fo + En + Chu; En + Chu + Fluid
MSH19	6.0	900	24	19/12	Fo + En + Chu; En + Chu + Fluid
MSH3	6.0	950	14	19/12	Fo + En + Chu; En + Chu + Fluid
MSH1	6.0	1,000	14	19/12	Fo + En + Chu; En + Chu + Fluid
MSH8	6.0	1,050	7	19/12	Fo + En + Chu; En + Chu + Fluid
MSH9	6.0	1,100	6	19/12	Fo + En + Fluid
MSH34	6.0	1,150	3	19/12	Fo + En + Melt
MSH28	6.0	1,200	4	19/12	Fo + En + Melt
MSH13	9.0	950	24	19/12	Fo + En + Chu; En + Chu + Fluid
MSH36	9.0	1,000	23	19/12	Fo + En + Cliu; En + Chu + Fluid
MSH22	9.0	1,050	7	19/12	Fo + En + Chu; En + Chu + Fluid
MSH35	9.0	1,100	4	19/12	Fo + En + Melt
MSH17	9.0	1,150	6	19/12	Fo + En + Melt
MSH58	10.5	850	2	18/11	A + En + Fluid
MSH39	10.5	1,150	3	18/11	Fo + En + Melt
MSH38	10.5	1,200	3	18/11	Fo + En + Melt[a]
MSH46	10.5	1,200	1	18/11	Fo + En + E[b]
MSH59	12.0	850	27	14/8	A + E + En; E + En + Chn; En + Fluid
MSH56	12.0	900	24	14/8	Fo + En + Chu; En + Fluid
MSH54	12.0	950	21	14/8	En + Chu + Chn
MSH50	12.0	1,000	1	14/8	Fo + En + Chu; En + Chu + Fluid[a]
MSH45	12.0	1,150	3	14/8	Fo + En + Melt
MSH52	13.0	1,000	14	14/8	E + En + Chu; En + Fluid[a]
MSH47	13.8	950	25	14/8	E + A; E + En; En + Fluid
MSH42	13.8	1,050	2	14/8	Fo + En + Chu; En + Fluid[a, c]
MSH53	13.8	1,100	5	14/8	E + En + Chu
MSH57	13.8	1,150	2	14/8	Fo + En + Melt[a]

[a] Quench plates and needles exhibited Raman spectra of phase E
[b] Run product was only studied by X-ray diffraction, E corresponds to quenched melt
[c] Optical distinction between fluid and melt was difficult

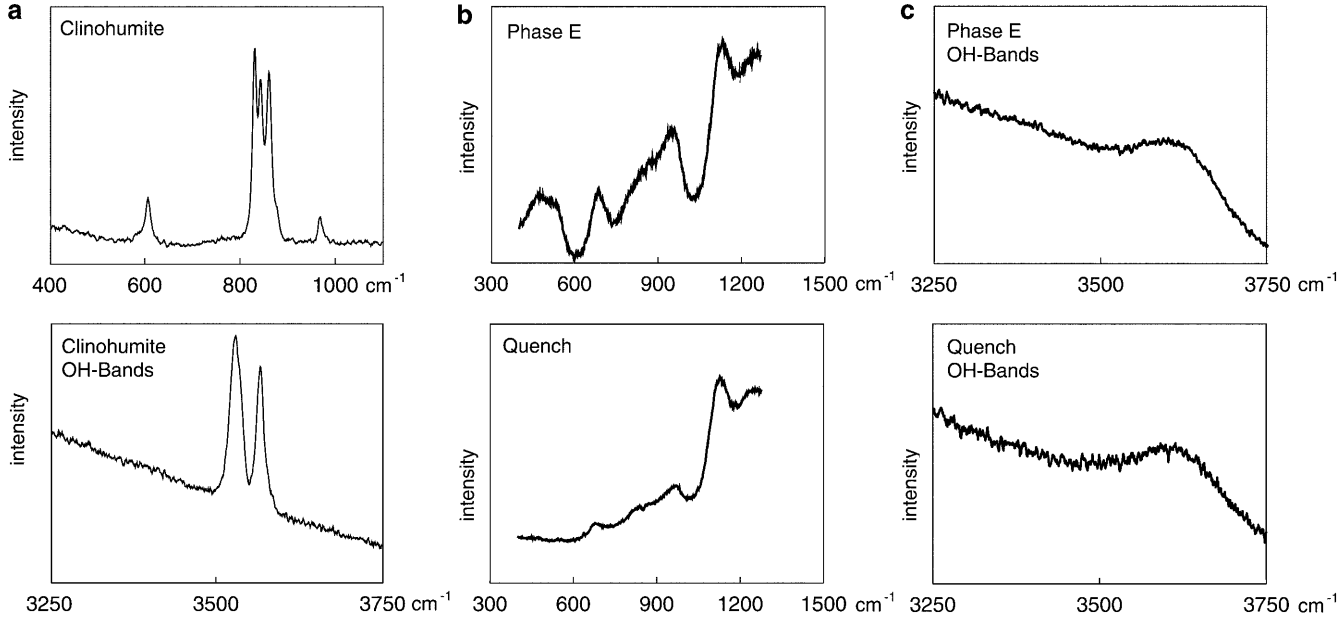

Fig. 2 Raman spectra of clinohumite and phase E. **a** Clinohumite exhibits three diagnostic peaks between 820 and 860 cm^{-1} and two OH-bands at 3,530 and 3,570 cm^{-1}. **b** Quench from hydrous fluids or melts shows exactly the same spectrum as phase E. Both quench and phase E do not show any sharp peak, probably owing to its unique crystal structure. **c** Broad OH-band of quench and of phase E, as observed previously by Ohtani et al. (1995) and Frost and Fei (1998)

presence of four different phases violates the phase rule (in a system with three components only three phases are allowed in a divariant field). However, the different phases were not distributed homogeneously throughout the capsule, and in most cases the four phases represent two different three-phase assemblages. The hydrous

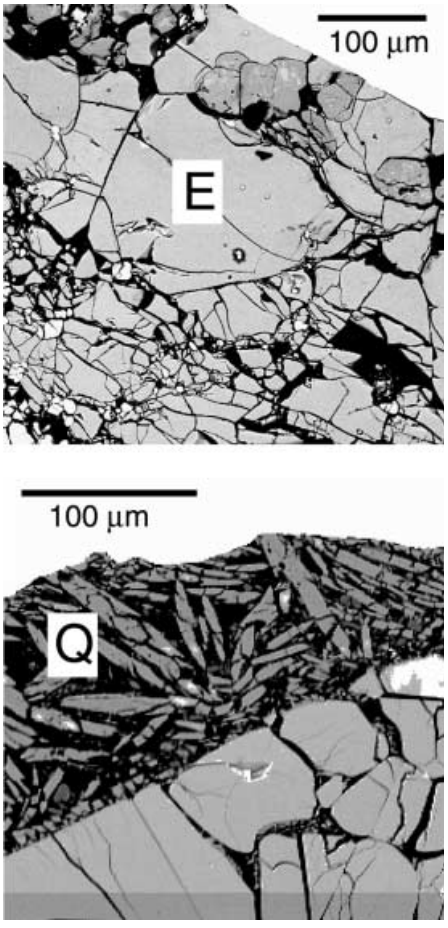

Fig. 3 BSE-image of stable phase E (*E*, *above*) and quench E (*Q*, *below*). Phase E was derived from run MSH47 and the quench from MSH38. Both phases exhibit identical Raman spectra and a very similar chemical composition (see text for discussion)

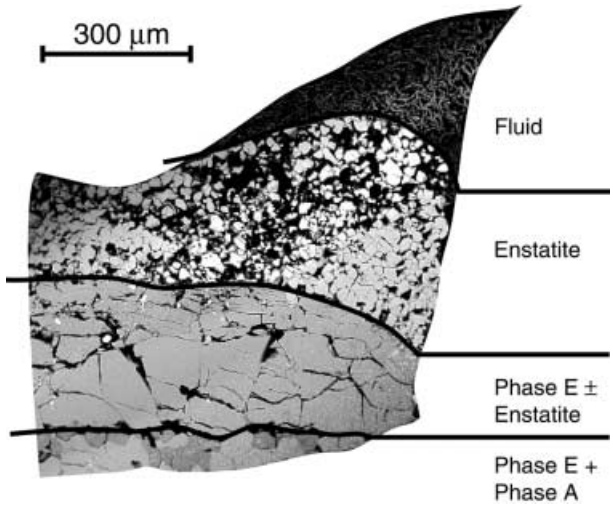

Fig. 4 BSE-image of run MSH47. Strong chemical zoning developed. Note that four phases occur (phase A, phase E, enstatite, fluid), but that they are not all in equilibrium with each other. Two three-phase assemblages can be deduced from this run: Phase A + Phase E + Enstatite and Phase E + Enstatite + Fluid (see Fig. 5)

fluid is concentrated at the top of the capsule and along the capsule wall (Figs. 4 and 5), and the hydrous solids occur preferentially at the bottom, sometimes also at the top of the charge. The centre of the capsule contains only anhydrous solids. In addition, all charges run above 10 GPa (i.e. with $LaCrO_3$ heaters) exhibit a Mg/Si gradient: Mg/Si at the bottom was much higher than in the centre. Capsules longer than 2 mm display symmetrical zoning. Both hydrous assemblage and quenched fluid have a Mg/Si ratio higher than forsterite. Hydrous fluid and anhydrous assemblage comprise in many cases by far the largest volume of the experimental charge. Thus hydrous phases such as clinohumite are easily overlooked and the stability field of enstatite + clinohumite underestimated.

Several possible mechanisms may contribute to the observed zonation:

1. Surface energy minimization. According to Watson (1999), fluids partition between different lithologies depending on the dihedral angle between fluid and minerals. A fluid gradient is expected to develop if the gain in surface energy exceeds the energy of the mineral reaction that is suppressed by the fluid gradient. If dihedral angles fall to values $< 60°$ an interconnected fluid network is formed, and the fluid can be expelled from the solid assemblage by compaction. Dihedral angles between fluid and Mg silicates decrease (and thus become more important as a driving force for phase separation) with increasing pressure and temperature (Watson et al. 1990; Mibe et al. 1999).

2. Density contrast. A low-density fluid can move upwards as long as a free fluid is stable under equilibrium conditions in the bulk system and an interconnected network is formed. Despite decreasing density contrasts with increasing pressure (high compressibility of the fluid, increasing amount of dissolved silicates) the aqueous fluid is the least dense phase under all conditions applied in this study.

3. Transport by fluid. Above 6 GPa aqueous fluids dissolve significantly more MgO than SiO_2 (Stalder et al. 2000). Thus, an increased H_2O content would accompany an enhanced Mg/Si ratio of the given sub-bulk system.

4. Thermal gradients (in particular for runs conducted with $LaCrO_3$ heaters). Soret diffusion can drive one component (i.e. Mg) towards low temperature and another component (i.e. Si) towards high temperature (centre of the capsule). Despite estimated thermal gradients lower than 10 °C/mm, this effect has to be taken into consideration, as capsules approaching the length of the stepped central part of the furnace show symmetrical zoning. The estimate of the temperature gradient is based on the observation that only one single experiment out of 30 runs evidenced the crossing of a reaction curve within the charge. This should have been observed much more often if temperature gradients were much higher, because the reaction curves above 10 GPa are often separated only by a few tens of degrees.

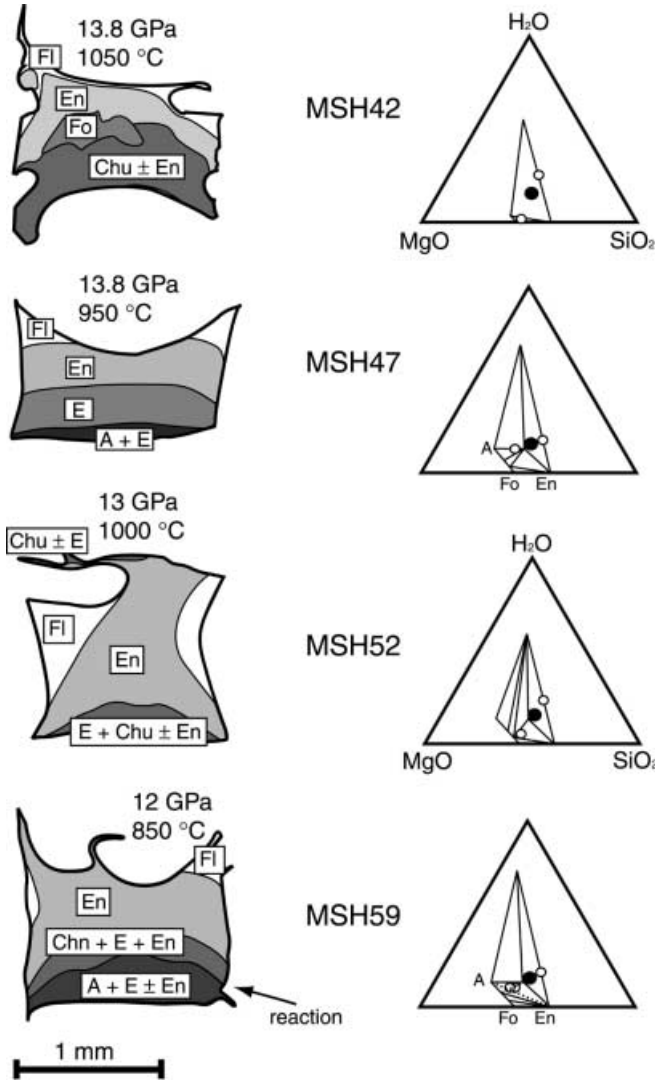

Fig. 5 Schematic drawings of longitudinal sections through the charges MSH42, 47, 52, 59 (*left column*). Clear zoning with respect to the fluid content and Mg/Si ratio developed, leading to different three-phase assemblages. In all cases four or five phases are formed. MSH59 (*bottom*) is a unique case, where four phases coexist stably, straddling the reaction curve Phase A + Enstatite → Phase E + Chondrodite. Zoned capsules cover cross sections over the MSH composition triangle (*right column*). *Filled dots* represent the starting composition [serpentine, $Mg_3Si_2O_5(OH)_4$], *open circles* show the estimated composition of the compositional domains

The Mg/Si ratio of the hydrous assemblage at the bottom of the capsule does not exceed that of the fluid. Therefore, both H_2O and Mg/Si distribution within the charges could be explained by transport in the fluid phase (point 3). If transport by the fluid is important, mechanisms 1 and 2 are prerequisite. If there is no driving force to move the fluid – either density contrast or fluid partitioning due to low wetting angles – the fluid would still dissolve silicates, but will not be able to transport them. In this context it is noteworthy that the reaction Phase *A* + *Enstatite* ⇔ *Chondrodite* + *PhaseE*, as observed in run MSH59 (Fig. 5), can only be explained by higher temperatures in the centre of the capsule (see discussion below). Probably all four mechanisms listed above are significant for our experiments. Due to the observed zonation of the run products, our study is not restricted to the serpentine system, but can be considered as a study within the system $MgSiO_3$–Mg_2SiO_4–$Mg(OH)_2$–H_2O, which covers the geologically most important part of the system MgO–SiO_2–H_2O. As the occurrence of more than three phases can be ascribed to the zonation (rather than real four-phase assemblages), the system can be treated as a three-component system.

Some run products at 5 and 6 GPa, however, locally do exhibit the coexistence of four phases (forsterite + enstatite + clinohumite + fluid), and clinohumites reach F-contents of up to 2 wt% (corresponding to $X_F = 0.33$). Thus for these pressures the system can be considered as a four-component system.

Selected microprobe analyses of hydrous phases are given in Table 3. In addition to the MSH components, the bulk system contained small amounts of other components, i.e. approximately 1 wt% FeO, 0.5 wt% Al_2O_3, 0.1 wt% F and 0.02 wt% TiO_2. None of the phases showed significant preference for incorporation of FeO and all phases revealed Mg# close to 99. Ti showed a preference for clinohumite and chondrodite. However, the amount of incorporated Ti is controlled by the amount of clinohumite or chondrodite, which in turn is controlled by the distribution of the major elements within the zoned capsule. Therefore Ti is considered as a trace element in all cases and is not expected to bias the phase assemblage. Al_2O_3 is concentrated in phase E or in the quench (as far as present). In a few experiments (all below 10 GPa) garnet was observed in minor amounts. Below 10 GPa F is concentrated in clinohumite. At 12 GPa and 950 °C (MSH54) chondrodite shows a slightly stronger preference for F than clinohumite, in accord to data at 0.2 GPa from Duffy and Greenwood (1979). The role of F for the stabilization of humite minerals and the role of Al for the stabilization of phase E will be discussed below.

Discussion

Two major differences to previous studies within the MSH system are notable: (1) phase E is not observed in our charges below 12 GPa (opposite to Luth 1995), and (2) a large stability field of clinohumite + enstatite develops at the expense of forsterite + fluid between 5 and 10 GPa.

Previous studies on the stability of phase E are mutually inconsistent. Several studies have indicated formation of phase E above 1,100 °C (Inoue et al. 1995; Luth 1995), whereas in other studies phase E was reported as a subsolidus phase that occurs between 800 and 1,100 °C (Kanzaki 1991; Kawamoto et al. 1995; Irifune et al. 1998). In our run products we observe that at low temperatures phase E forms large euhedral crystals (Fig. 3) with slightly greenish colour. However, quench blades and quench needles from fluids and melts

Table 3 Microprobe analyses of hydrous phases. *Qu* Quench, *n.d.* not detected, *n.a.* not analysed. Water contents for phase A, E and Quench were calculated by difference to 100 wt%. Water contents for Chu and Chn were calculated from their Ti and F-contents. Qu from MSH47 was very fine grained and analysed with rastered beam

Run no.	Phase	Points	MgO		SiO_2		Al_2O_3		FeO		TiO_2		Mg#		(Mg + Fe)/Si		F		H_2O
			wt%	SD	wt%	SD	wt%	SD	wt%	SD	wt%	SD	–	SD	–	SD	wt%	SD	wt%
MSH59	A	6	58.83	0.29	26.33	0.21	0.10	0.00	1.43	0.06	n.d.	–	98.65	0.06	3.38	0.03	n.d.	–	13.30
MSH47	A	3	60.23	0.63	26.79	0.09	0.03	0.01	0.35	0.08	n.d.	–	99.68	0.07	336	0.03	0.24	0.15	12.38
MSH59	E	6	46.70	0.25	38.41	0.33	3.32	0.08	1.25	0.07	0.04	0.02	98.52	0.07	1.84	0.01	n.d.	–	10.27
MSH52	E	3	48.18	0.28	39.29	0.34	2.19	0.06	1.42	0.01	0.03	0.03	98.38	0.02	1.86	0.01	n.d.	–	8.89
MSH47	E	8	49.29	0.39	38.43	0.39	0.81	0.12	1.62	0.14	n.d.	–	98.19	0.16	1.95	0.02	n.d.	–	9.85
MSH38	Qu	9	47.63	0.86	36.49	1.97	n.a.	–	n.a.	–	–	–	–	–	–	–	–	–	–
MSH45	Qu	6	48.80	0.58	39.67	0.69	1.95	0.17	1.15	0.06	0.06	0.04	98.69	0.08	1.86	0.05	n.a.	–	8.36
MSH47	Qu	6	34.31	15.25	18.49	9.54	0.63	0.37	1.27	0.66	n.d.	–	98.03	0.29	2.98	0.50	n.a.	–	45.09
MSH42	Qu	7	45.75	2.08	33.52	2.50	2.89	0.23	1.88	0.19	n.d.	–	97.74	0.21	2.09	0.10	n.a.	–	15.94
MSH59	Chn	7	57.03	0.22	34.87	0.23	0.03	0.01	1.16	0.04	0.21	0.05	98.87	0.04	2.47	0.02	1.21	0.35	4.67
MSH54	Chn	17	57.58	0.62	35.59	0.90	0.06	0.01	1.58	0.17	0.05	0.05	98.49	0.17	2.45	0.05	0.22	0.04	5.18
MSH49	Chu	12	56.92	0.42	39.32	0.47	0.06	0.05	1.16	0.05	0.20	0.07	98.86	0.06	2.18	0.04	1.60	0.28	2.09
MSH51	Chu	4	57.38	0.21	38.48	0.79	0.07	0.01	1.16	0.05	0.34	0.03	98.87	0.05	2.25	0.05	1.99	0.10	1.87
MSH55	Chu	9	56.30	0.54	38.53	0.57	0.04	0.03	1.37	0.21	n.d.	–	98.66	0.20	2.21	0.02	n.a.	–	–
MSH13	Chu	10	57.66	0.61	38.88	0.40	0.06	0.02	1.24	0.06	0.09	0.03	98.81	0.06	2.24	0.03	0.60	0.06	2.59
MSH56	Chu	6	58.02	0.37	38.68	0.38	0.05	0.02	1.25	0.06	0.08	0.04	98.81	0.05	2.26	0.01	0.12	0.03	2.82
MSH54	Chu	7	57.05	0.49	38.68	0.47	0.06	0.03	1.25	0.05	0.03	0.03	98.78	0.03	2.23	0.04	0.09	0.05	2.85
MSH50	Chu	9	56.95	0.68	38.12	0.47	0.13	0.02	1.22	0.05	0.04	0.03	98.82	0.05	2.25	0.03	0.12	0.04	2.83
MSH52	Chu	5	58.10	0.29	38.62	0.19	0.05	0.02	1.07	0.05	0.07	0.05	98.98	0.05	2.27	0.01	0.16	0.06	2.80
MSH42	Chu	6	57.34	0.13	38.32	0.44	0.09	0.02	1.23	0.02	0.09	0.06	98.81	0.02	2.26	0.03	0.31	0.09	2.73

above 10 GPa show exactly the same Raman spectrum (Fig. 2b, c), chemical composition (Table 3) and X-ray pattern (compare runs MSH38 and MSH46, both 10.5 GPa and 1,200 °C, Table 2) as phase E. Therefore, we conclude that the true stability field of phase E can only be determined when textural observations are included. X-ray powder diffraction analysis alone most probably leads to an overestimation of the stability field of phase E, as no distinction between quench and stable phases can be made.

Taking into account all observations described above we performed a Schreinemakers' analysis with the existing data. It has to be noted that the phase diagram is based on forward synthesis experiments, and no attempt has been made to reverse the experiments. The strong zonation of the experimental charges was advantageous as some runs covered entire cross sections through the MSH composition triangle (Fig. 5). Experimental runs and observed tie lines are shown in Fig. 6a, and numbered reaction curves in Fig. 6b and Table 4. Run MSH59 (12 GPa, 850 °C) is of particular interest. In the lower half of the capsule section two three-phase assemblages (Phase A + Phase E + Enstatite and Chondrodite + Phase E + Enstatite) with similar bulk composition are juxtaposed. The latter paragenesis is closer to the centre of the furnace and experienced thus slightly higher temperatures, in accord with Schreinemakers' analysis. Therefore this run can be regarded as direct observation of reaction (11) (Phase A + Enstatite↔Chondrodite + Phase E) and represents an accurate bracket for this reaction in the P–T plot (Fig. 6b).

Previous investigators determined nearly identical conditions for the breakdown of enstatite + phase A [reaction (1); Luth 1995], and the formation reaction of clinohumite from forsterite + phase A [reaction (2); Wunder 1998] between 7 and 10 GPa. Within this pressure range the invariant point (I) is located in the pure MSH system; on the high pressure side of (I) reaction (4) (Enstatite + Phase A ↔ Clinohumite + Fluid) takes place.

Since reactions (1) and (2) are located within a very narrow temperature interval clinohumite only occurs within a thin band and may have been overlooked by some investigators. In the MSH system the assemblage clinohumite + enstatite has previously been observed only between 9 and 13 GPa (Kanzaki 1991; Kawamoto et al. 1995; Luth 1995). The temperature difference between the breakdown of enstatite + phase A [reaction (4)] and the breakdown of enstatite + clinohumite to forsterite + fluid [reaction (3)] increases with increasing pressure (Fig. 6c).

The most important differences between pure MSH and the F- and Al-containing system (Fig. 6c) are the drastically increased thermal stability of clinohumite, the occurrence of chondrodite between 9 and 12 GPa and the formation of phase E towards lower pressures. All these features are due to the selective incorporation of aluminium in phase E and of fluorine in the humite minerals. With increasing pressure F-contents in

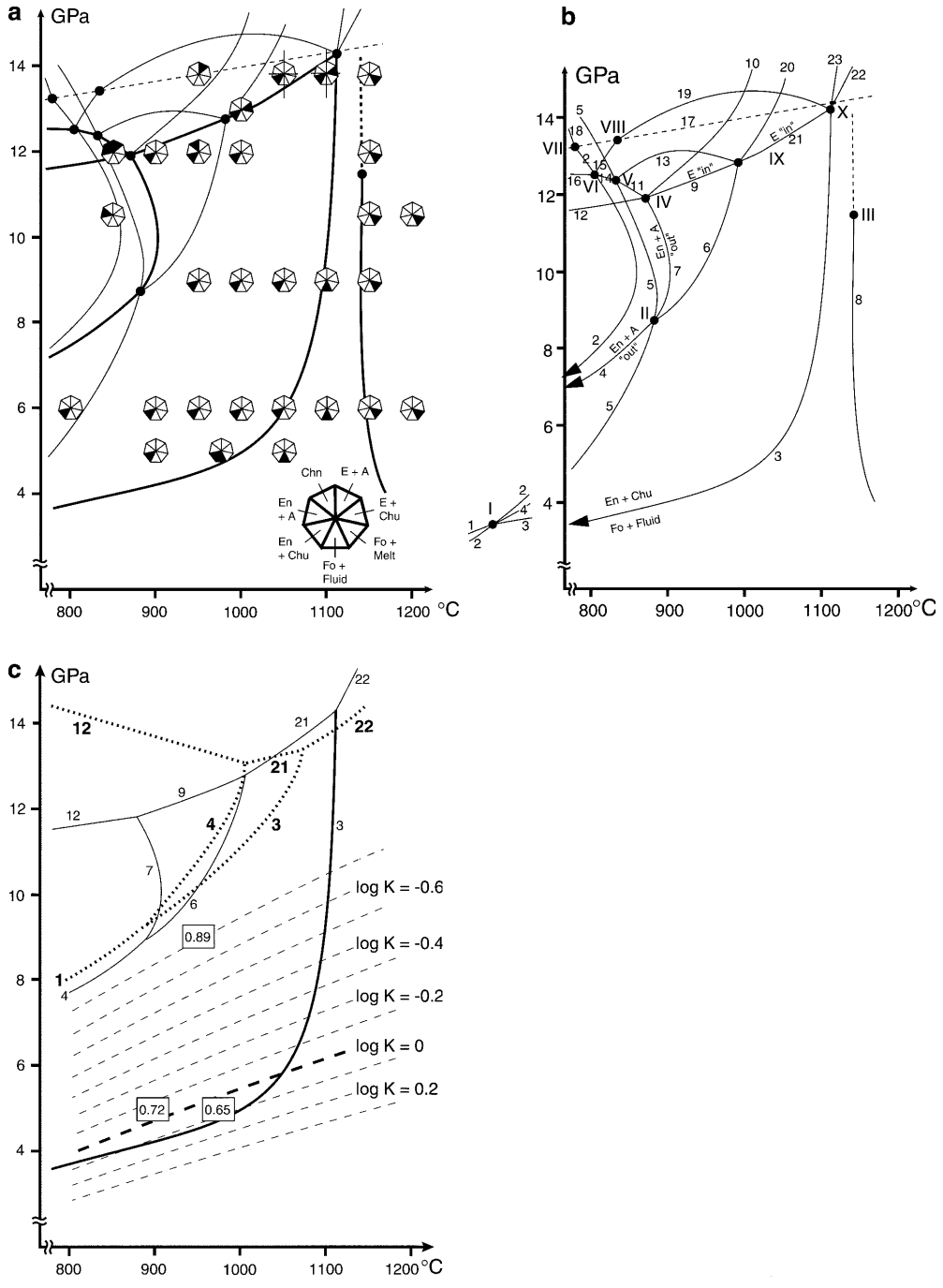

Fig. 6 **a** Pressure–temperature diagram of high pressure experiments. *Filled sectors* of each symbol indicate observed assemblages under run conditions respectively. Over a wide range the assemblage clinohumite + enstatite (and therefore forsterite + enstatite + clinohumite) is stable. *Solid dots* represent invariant points where five reaction curves meet. The thermal decomposition of clinohumite occurs below the mantle solidus. Above 12 GPa the distinction between fluid and melt is arbitrary. *Error bars* for uncertainties of the experimental conditions are depicted for two 13.8 GPa runs, and apply to all other experiments too. **b** Reactions and invariant points (see Table 4) determined by Schreinemaker's analysis. **c** Comparison of data from this study (*solid lines*) with the pure MSH system (*dotted lines*). *Labelled reactions* refer to Table 4. Reactions (1), (3) and (4) below 11 GPa are taken from Luth (1995), (4), (12) and (21) from Kanzaki (1991). *Broken lines* correspond to reaction (3), 0.5 enstatite + clinohumite $\leftrightarrow$ 5 forsterite + H_2O, calculated for different Ks with the thermodynamic data of Holland and Powell (1998). *Numbers in boxes* indicate the X_{OH} of the stable clinohumite. Above 10 GPa X_{OH} range between 0.94 and 0.98

the clinohumite decrease drastically, and the two phase diagrams become more similar. The same is valid above 1,000 °C for reactions involving phase E. Reactions devoid of humite minerals or phase E (not shown in Fig. 6c) are not affected by the presence of Al or F, as incorporation of these elements in phases other than phase E and the humite minerals is negligible (Table 3).

As illustrated in Fig. 6c, reaction (3), *enstatite + clinohumite* $\Leftrightarrow$ *forsterite* + H_2O, was calculated with the thermodynamic data of Holland and Powell (1998). Decreasing activities of both clinohumite and H_2O were taken into account by changing the reaction constant K. Decreased activity of H_2O due to dissolved silicate components (logK > 0) shifts the reaction curve towards higher pressure (lower temperature). Conversely, if the clinohumite deviated from its pure OH end member, the reaction is shifted towards lower pressure (higher temperature). The curve for logK = 0 (pure phases) matches quite well with the reaction curve observed in our study up to 1,050 °C, but not the reaction in the pure MSH system. Most probably, this mismatch is caused by the limited accuracy of the available thermodynamic data for hydrous silicates and the high pressure hydrous

Table 4 Reactions and invariant points

Invariant points:	
I	Fo, En, Chu, A, Fluid
II	En, Chu, Chn, A, Fluid
III	Fo, En, Fluid, Melt (termination of the solidus)
IV	En, Chn, A, E, Fluid
V	En, Chu, Chn, A, E
VI	Fo, En, Chu, A, E
VII	Fo, Wd, Chu, A
VIII	Fo, Wd, En, Chu, E
IX	En, Chu, Chn, E, Fluid
X	Fo, En, Chu, E, Fluid
1	Fo + Fluid = En + A
2	Fo + A = Chu
3	Fo + Fluid = En + Chu
4	En + A = Chu + Fluid
5	Chu + A = Chn
6	En + Chn = Chu + Fluid
7	En + A = Chn + Fluid
8	Fo + Fluid ± En = Melt ± En (eutectic to peritectic)
9	En + Chn + Fluid = E
10	A + E = Chn + Fluid
11	En + A = Chn + E
12	En + A + Fluid = E
13	En + Chn = Chu + E
14	En + A = Chu + E
15	En + Chu = Fo + E
16	En + A = Fo + E
17	Fo = Wd
18	Wd + A = Chu
19	En + Chu = Wd + E
20	Chn + E = Chu + Fluid
21	En + Chu + Fluid = E
22	Mg_2 SiO_4 + En + Fluid = E
23	Chu + E = Mg_2SiO_4 + Fluid

fluids. For example, in all reactions involving a hydrous fluid, only pure H_2O is taken into account. Furthermore, thermodynamic data for pure H_2O are derived from 'dehydration' reactions at high pressure and temperature (Brodholt and Wood 1993), where the fluid produced by the breakdown is highly charged with oxide components. Considering continuously decreasing activities of H_2O in the fluid with increasing temperature, the shape of reaction (3) can be reconciled: The breakdown of clinohumite (both on its own composition and coexisting with enstatite) has a positive P–T slope. With increasing P and T enhanced silicate solubility in the fluid reduces the activity of H_2O in the fluid continuously. Instead of a single reaction curve, reaction (3) rather represents a bundle of reaction curves with decreasing logK at increased P and T. Such a continuous decrease of the H_2O activity with increasing temperature (and pressure) might be a viable explanation for the breakdown of clinohumite to forsterite + periclase + fluid reported by Yamamoto and Akimoto (1977) and Pawley (2000) respectively. Experimental data below 3 GPa can be well fitted up to 1,000 °C (Pawley 2000). However, extrapolation of this fit towards higher temperature fails to match experimental results of Yamamoto and Akimoto (1977) up to 7.7 GPa, where the breakdown of OH-clinohumite has been observed below 1,200 °C – hundreds of degrees below the extrapolated breakdown.

With respect to the stability of clinohumite + enstatite our results contradict some previous studies on serpentine composition (e.g. Irifune et al. 1996, 1998), where no clinohumite was observed. However, these studies focused on much higher pressures (most runs were between 10 and 25 GPa) and a much broader range of temperature (25–1,400 °C). Furthermore differences in the starting composition might be crucial [Irifune et al. (1996, 1998) do not report the F- and Ti-contents of their bulk composition.] The opposing results of the few runs obtained by the previous studies that plot within the clinohumite stability field inferred from the present study might also be ascribed to the chemical zonation described in the section above.

The mechanism of formation of OH-clinohumite and OH-chondrodite in the present study may have been a complicated process. Minerals belonging to the humite family (e.g. clinohumite and chondrodite) tend to form polysomatic series (White and Hyde 1982). In addition, the incorporation of water into olivine is isostructural with the OH-rich interlayer of the humite group mineral (Drury 1991; Risold et al. 2000). It cannot be excluded that to a certain degree polysomes formed, as irregularities of lattice spacings parallel to (001) can only be identified with high resolution transmission electron microscopy. However, electron microprobe analyses revealed chemical compositions close to stoichiometry. Run products from MSH49 and MSH55 were very fine grained (usually only a few micrometre grain size), and it cannot be excluded that deviations from stoichiometry of clinohumites from these runs are analytical artefacts biased by neighbouring enstatite or forsterite grains.

Subduction of water into the transition zone

The stability of Ti-clinohumite in a mantle assemblage has been proposed earlier in Ti-rich bulk compositions (Khodyrev et al. 1992; Iizuka and Nakamura 1995), and indeed Ti-clinohumite and Ti-chondrodite are found in natural rocks of mantle origin (Aoki et al. 1976; Ribbe 1980). Our observations suggest that small amounts of F are sufficient to increase the stability of clinohumite and chondrodite considerably and that the presence of F can be considered crucial for the survival of humite minerals (Evans and Trommsdorff 1983) during metamorphism. Chondrodite never represents the only stable hydrous phase (Fig. 6b), and its occurrence is limited to parageneses with more than 2 wt% water. Clinohumites with similar F-contents as observed in our experiments at 5 GPa occur in ultramafic rocks of Cima di Gagnone (Ticino/Switzerland; Evans and Trommsdorff 1983), which experienced high pressure metamorphism (2.5 GPa, 800 °C). Considering that the F/OH ratio of clinohumite decreases drastically with increasing pressure, as shown in our experiments, clinohumites such as the ones reported from Cima di Gagnone would have survived much higher pressures.

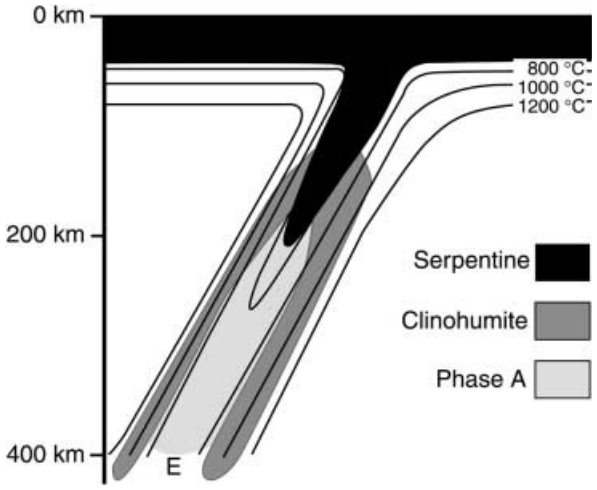

Fig. 7 Thermal structure of a subduction zone with a subduction angle of 60° and a plate velocity of 4.5 cm/year (after Davies and Stevenson 1992). The different fields show the stability of serpentine, clinohumite and phase A in peridotitic rocks respectively. At depths between of 120 and 180 km serpentine decomposes forming clinohumite, enstatite and fluid. Clinohumite persists to the top of the transition zone (400 km depth). At still greater depth water can be stored in phase E. OH-chondrodite is not considered here, as it is only formed if the water content of the assemblage exceeds 2 wt%

The stability of clinohumite in mantle rocks over a wide range of pressure and temperature conditions has important implications for the transport of water into the Earth's mantle. Figure 7 shows a cross section through a subduction zone, with the stability fields of serpentine, phase A and clinohumite in peridotite superimposed on the thermal structure (Davies and Stevenson 1992). Given the thermal gradients implied by Fig. 7, serpentine decomposes continuously down to a depth of about 200 km. To depths of 120 km, dehydration of serpentine produces forsterite + enstatite ± chlorite + fluid; between 120 and 180 km clinohumite, enstatite and fluid are formed, and at still greater depths the remaining serpentine decomposes to phase A, enstatite and fluid. Water released between 120 and 180 km could move upwards and stabilize clinohumite in parts of the overlying mantle. By this mechanism, water stored in the peridotitic part of the subducted oceanic lithosphere and additional water located in the overlying mantle wedge could be dragged down into the transition zone (= 400 km). The 'choke point' located at approximately 6 GPa and 600 °C, above which H_2O can no longer be transported in mineral phases, is shifted to much higher P and T and the potential storage and transport capacity for H_2O in the subduction zone could thereby be greatly increased.

Both phase A and clinohumite become unstable above 12 to 14 GPa for peridotitic bulk composition and are replaced by the assemblage phase E + forsterite + enstatite. This reaction occurs near the α–β-Mg_2SiO_4 transition (Fig. 6a), which is responsible for the 400 km seismic discontinuity (Akimoto et al. 1976; Katsura and Ito 1989). OH-clinohumite contains only 2.9 wt% H_2O (compared to 13 wt% H_2O in serpentine), and a plausible hydrated mantle assemblage forsterite + enstatite + clinohumite contains no more than 1 wt% (compared to 8–9 wt% in completely hydrated serpentinite). Therefore, at relatively shallow depth of subduction, most of the water subducted with the hydrated oceanic lithosphere will be released to the mantle wedge to serve as a flux for the generation of island-arc magmas. However, about 10% of the initially subducted water could be carried into the Earth's transition zone and probably into the lower mantle. The high thermal stability of clinohumite in a system containing small amounts of fluorine implies that subduction of water into the transition zone is potentially a widespread process (i.e. not restricted to the coldest spot of the subducted slab).

Acknowledgements This project was kindly supported by the Schweizer Nationalfond, grant 2000-050661.97. We gratefully acknowledge Eric Reusser and Ralf Kägi for assistance with microprobe analyses and Jamie Connolly for help with the thermodynamic calculations and helpful comments on an earlier version of this manuscript. Anne-Chantal Risold and Alison Pawley are thanked for valuable discussion and communication about their work and Bernard Evans, Martin Engi and an anonymous reviewer for their prompt and thorough reviews.

References

Akaogi M, Susaki J-I, Yagi T, Matsui M, Kikegawa T, Yusa H, Ito E (1992) High pressure–temperature stability of a PbO_2-type TiO_2 and $MgSiO_3$ majorite; calorimetric and in situ diffraction studies. In: Syono Y, Mangnani MH (eds) High pressure research: application to earth and planetary sciences. Geophys Monogr 67:447–455

Akimoto S, Akaogi M (1980) The system Mg_2SiO_4–MgO–H_2O at high pressures and temperatures – possible hydrous magnesian silicates in the mantle transition zone. Phys Earth Planet Inter 23:268–275

Akimoto S, Matsui Y, Syono Y (1976) High-pressure crystal chemistry of orthosilicates and formation of the mantle transition zone. In: Sterns RGJ (ed) The physics and chemistry of rocks. Wiley, London, pp 327–363

Aoki K, Fujino K, Akaogi M (1976) Titanochondrodite and titanoclinohumite derived from the upper mantle in the Buell Park kimberlite, Arizona, USA. Contrib Mineral Petrol 56:243–253

Bose K, Navrotsky A (1998) Thermochemistry and phase equilibria of hydrous phases in the system MgO–SiO_2–H_2O: implications for volatile transport to the mantle. J Geophys Res 103B:9713–9719

Brodholt J, Wood B (1993) Simulations of the structure and thermodynamic properties of water at high pressures and temperatures. J Geophys Res 98B:519–536

Chinnery NJ, Pawley AR, Clark SM (1999) In situ observation of the formation of 10 Å phase from talc + H_2O at mantle pressures and temperatures. Science 286:940–942

Davies JH, Stevenson DJ (1992) Physical model of source region of subduction zone volcanism. J Geophys Res 97:2037–2070

Drury MR (1991) Hydration induced climb dissociation of dislocations in naturally deformed mantle olivine. Phys Chem Miner 18:106–116

Duffy CF, Greenwood HJ (1979) Phase equilibria in the system MgO–MgF_2–SiO_2–H_2O. Am Mineral 64:1156–1174

Evans BW, Trommsdorff V (1983) Fluorine hydroxyl titanian clinohumite in alpine recrystallized garnet peridotite: compositional controls and petrologic significance. Am J Sci 283A:355–369

Frost DJ, Fei Y (1998) Stability of phase D at high pressure and high temperature. J Geophys Res 103:7463–7474
Hofmeister AM, Cynn H, Burnley PC, Meade C (1999) Vibrational spectra of dense, hydrous magnesium silicates at high pressure: importance of the hydrogen bond angle. Am Mineral 84:454–464
Holland TJB, Powell R (1998) An internally consistent thermodynamic data set for phases of petrological interest. J Metamorph Geol 16:309–343
Iizuka Y, Nakamura E (1995) Experimental study of the slab–mantle interaction and implications for the formation of titanoclinohumite at deep subduction zone. Proc Jpn Acad 71B:159–164
Inoue T, Yurimoto H, Kudoh Y (1995) Hydrous modified spinel, $Mg_{1.75}SiH_{0.5}O_4$: a new water reservoir in the mantle transition region. Geophys Res Lett 22:117–120
Irifune T, Kuroda K, Funamori N, Uchida T, Yagi T, Inoue T, Miyajima N (1996) Amorphization of serpentine at high pressure and high temperature. Science 272:1468–1470
Irifune T, Kubo N, Isshiki M, Yamasaki Y (1998) Phase transformations in serpentine and transportation of water into the lower mantle. Geophys Res Lett 25:203–206
Kanzaki M (1991) Stability of hydrous magnesium silicates in the mantle transition zone. Phys Earth Planet Inter 66:307–312
Katsura T, Ito EJ (1989) The system Mg_2SiO_4–Fe_2SiO_4 at high pressures and temperatures: precise determination of stabilities of olivine, modified spinel, and spinel. J Geophys Res 94B(11):15663–15670
Kawamoto T, Leineweber K, Hervig RL, Holloway JR (1995) Stability of hydrous minerals in H_2O-saturated KLB-1 peridotite up to 15 GPa. In: Farley KA (ed) Volatiles in the earth and solar system. Am Inst Phys, New York, pp 229–239
Khodyrev OY, Agoshkov VM, Slutskiy AB (1992) The system peridotite–aqueous fluid at upper mantle parameters. Trans USSR Acad Sci: Earth Sci Sect 312:255–258
Liu L (1987) Effects of H_2O on the phase behaviour of the forsterite–enstatite system at high pressures and temperatures and implications for the Earth. Phys Earth Planet Inter 49:142–167
Liu L, Lin CC, Mernagh TP, Irifune T (1997a) Raman spectra of phase A at various pressures and temperatures. J Phys Chem Solids 58:2023–2030
Liu L, Mernagh TP, Lin CC, Irifune T (1997b) Raman spectra of phase E at various pressures and temperatures with geophysical implications. Earth Planet Sci Lett 149:57–65
Luth RW (1995) Is phase A relevant to the Earth? Geochim Cosmochim Acta 59:679–682
Mibe K, Toshitsugu F, Yasuda A (1999) Control of the location of the volcanic front in island arcs by aqueous fluid connectivity in the mantle wedge. Nature 401:259–262
Morishima H, Kato T, Suto M, Ohtani E, Urakawa S, Utsumi W, Shimomura O, Kikegawa T (1994) The phase boundary between α and β-Mg_2SiO_4 determined by in situ X-ray observation. Science 265:1202–1203
Ohtani E, Shibata T, Kubo T, Kato T (1995) Stability of hydrous phases in the transition zone and the upper most part of the lower mantle. Geophys Res Lett 22:2553–2556
Pawley A (2000) Stability of clinohumite in the system MgO–SiO_2–H_2O. Contrib Mineral Petrol 138:284–291
Ribbe PH (1980) The humite series and Mn-analogs. In: Ribbe PH (ed) Orthosilicates. Rev Mineral 5:231–274
Ringwood AE, Major A (1967) High pressure reconnaissance investigations in the system Mg_2SiO_4–MgO–H_2O. Earth Planet Sci Lett 2:130–133
Risold AC, Trommsdorff V, Grobéty B (2000) Genesis of ilmenite rods and palisades along humite-type defects in olivine from Alpe Arami. Contrib Mineral Petrol (in press)
Stalder R, Ulmer P, Thompson AB, Günther D (2000) High pressure fluids in the system MgO–SiO_2–H_2O at upper mantle conditions. Contrib Mineral Petrol (in press)
Susaki JI, Akaogi M, Akimoto S, Shimomura O (1985) Garnet–perowskite transformation in $CaGeO_3$: in-situ X-ray measurements using synchrotron radiation. Geophys Res Lett 12:729–732
Ulmer P, Trommsdorff V (1995) Serpentine stability to mantle depths and subduction- related magmatism. Science 268:858–861
Watson EB (1999) Lithologic partitioning of fluids and melts. Am Mineral 84:1693–1710
Watson EB, Brenan JM, Baker DR (1990) Distribution of fluids in the continental mantle. In: Menzies MA (ed) Continental mantle. Oxford Monogr Geol Geophys 16:111–125
White TJ, Hyde BG (1982) Electron microscope study of humite minerals: I. Mg-rich specimens. Phys Chem Miner 8:55–63
Wunder B (1998) Equilibrium experiments in the system MgO–SiO_2–H_2O (MSH): stability fields of clinohumite-OH [$Mg_9Si_4O_{16}(OH)_2$], chondrodite-OH [$Mg_5Si_2O_8(OH)_2$] and phase A [$Mg_7Si_2O_8(OH)_6$]. Contrib Mineral Petrol 132:111–120
Yagi T, Akimoto S (1976) Direct determination of coesite–stishovite transition by in-situ X-ray measurements. Tectonophysics 35:259–270
Yamamoto K, Akimoto S (1977) The system MgO–SiO_2–H_2O at high pressures and temperatures – stability field for hydroxyl-chondrodite, hydroxyl-clinohumite and 10Å-phase. Am J Sci 277:288–312
Zhang J, Li B, Utsumi W, Liebermann RC (1996) In situ X-ray observations of the coesite–stishovite transition: reversed phase boundary and kinetics. Phys Chem Miner 23:1–10